Chirality Specific Triplet Exciton Dynamics in Highly Enriched (6,5) and (7,5) Carbon Nanotube Networks

Abasi Abudulimu,[a] *Florian Spaeth,*[b] *Imge Namal,*[b] *Tobias Hertel,*[b] *Larry Lüer*,*[a]

[a] IMDEA Nanociencia, C/ Faraday 9, 28049 Cantoblanco, Madrid, Spain.

[b] Institute of Physical and Theoretical Chemistry, Julius-Maximilian University Würzburg, Germany

Supporting Information:

Table of contents:

A Ground state absorption spectra and determination of chirality concentration

Fig. S1 shows ground state absorption ("abs", upper row) for the (6,5) rich and the (7,5) rich sample (left and right column, respectively). The absorption spectra are dominated by intense

bands at 1.24 and 1.19 eV referring to the E11 excitonic transition of the (6,5) and (7,5) tubes (dots in Fig. 1a and b, respectively). Weaker maxima are associated with the presence of other chiralities. We calculated the relative spectral weights of SWNT chiralities in our samples by fitting the ground state absorption spectra by a superposition of Gaussians and taking the area under each individual absorption peak to represent the relative nanotube chirality concentration in the sample [1]. In order to properly fit the absorption spectra (red curves), we had to include several chiralities, as indicated in the figure. The linewidths of (6,5) and (7,5) E11 excitonic bands were determined from (6,5) and (7,5) rich samples (which are 34meV and 24meV, respectively), and fixed in the model, while the other linewidths are limited between 20meV and 40meV. Fig. S1 (red curves in upper row), shows the fit results of ground state absorption spectra, as well as the corresponding relative chirality concentration in both (6,5) and (7,5) rich samples (gray bars in panel c and d). Assuming a chirality-independent absorption cross section, we found that the (6,5) rich sample contains about 92% of (6,5) tubes and about 2% of (7,5) tubes, while the (7,5) rich sample contains about 78% (7,5) tubes and about 7% of (6,5) tubes. Most of the remaining tubes are on the lower energy side in both samples, so that it is in principle possible to observe energy and charge transfer processes.

The wavelength of the pump pulse in these experiments was 387 nm (3.204 eV), which essentially excites the free carrier background of all chiralities leading to a chirality unspecific generation of electron-hole pairs. Within the duration of the pump pulse, the electron hole pairs are expected to localize to form bound excitons [2-6] causing a transient photobleach (PB) of the corresponding absorption feature. To see if the excited states remain in the most abundant chirality soon after the pump pulse is off, we conducted the spectral fit procedure also on transient absorption spectra of both (6,5) and (7,5) rich samples recorded at 0ps (the time resolution in our system is approximately 150fs). Fig.S1 (c and d), shows the transient absorption (TA) spectra (dots) and the fit results (lines), as well as the corresponding relative spectral weights of chiralities (yellow bars) in both (6,5) and (7,5) rich samples. Comparing the early time TA spectra with the ground state absorption spectra, we found for both samples that the lower energetic PB features are relatively stronger than the corresponding ground state absorption features, which is rendered in the bar graphs as well, compare yellow shaded and grey shaded bars, respectively. This can either be caused by ultrafast downhill energy transfer in

hexagonal aggregates, which has been shown to occur on a 10 fs time scale [4] and thus during our 150 fs pump pulse, or it can be caused by a relatively stronger oscillator strength of the free carrier continuum of the lower energetic tubes compared to the (6,5) tube. In any case, we note that at the end of the 150 fs pump pulse, most of the excited states reside on the dominant tubes (on (6,5) tubes in the (6,5) rich sample, and on (7,5) tubes in the (7,5) rich sample). We discard any high-intensity effects as reason for the observed over-representation of low energy tubes in the TA spectra, since the pump intensity dependence of the effect is weak and in the opposite direction (see table S1 and S2). In the TA spectra, the lower energetic PB bands are superposed with a large photoinduced absorption band of opposite sign, which has been assigned to excited state absorption of the (6,5) or (7,5) singlet exciton $PA_E^{6,5}$ or $PA_E^{7,5}$ [7-8], so we consider the start of our experiment as characterized by a large excess of singlet excitons on (6,5) or (7,5) tubes in the respective samples.

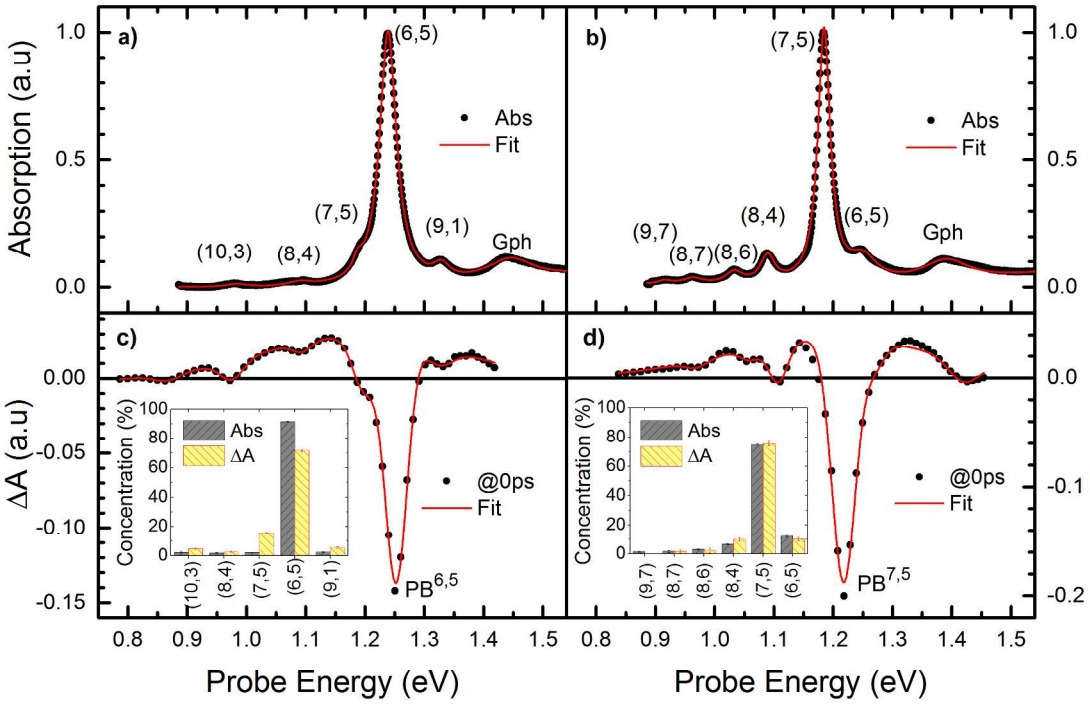

Fig.S1 Ground state absorption (upper panel) and TA spectra (lower panel) of (6,5) (left column) and (7,5) (right column) rich SWNT samples. The insets in c) and d) are the SWNT chirality distributions in the respective samples, where Abs refers to ground state absorption spectra, ΔA refers to transient absorption spectra and the numbers with brackets in the X axes refer to chirality indices.

Table S1. Pump intensity dependence of relative spectral weights in the (6,5) rich sample

33 μJ/cm^2			99 μJ/cm^2		198 μJ/cm^2	
Chirality	**Spectral weight, %**	**Error**	**Spectral weight, %**	**Error**	**Spectral weight, %**	**Error**
(10,3)	4.74E+00	5.69E-01	3.77E+00	9.35E-01	2.99E+00	4.51E-01
(8,4)	2.47E+00	5.79E-01	1.58E+00	5.70E-01	8.46E-01	4.63E-01
(7,5)	1.57E+01	6.60E-01	1.54E+01	7.53E-01	1.55E+01	5.37E-01
(6,5)	7.15E+01	6.82E-01	7.46E+01	1.33E+00	7.72E+01	5.52E-01
(9,1)	5.52E+00	6.69E-01	4.65E+00	6.58E-01	3.54E+00	5.35E-01

Table S2. Pump intensity dependence of relative spectral weights in (7,5) rich sample

33 μJ/cm^2			99 μJ/cm^2		198 μJ/cm^2	
Chirality	**Spectral weight, %**	**Error**	**Spectral weight, %**	**Error**	**Spectral weight, %**	**Error**
(10,3)	1.77E+00	1.28E+00	1.56E+00	1.27E+00	1.14E+00	1.25E+00
(8,4)	2.52E+00	1.84E+00	2.46E+00	1.88E+00	2.26E+00	1.73E+00
(7,5)	9.92E+00	1.23E+00	8.47E+00	1.28E+00	7.41E+00	1.18E+00
(6,5)	7.55E+01	1.59E+00	7.78E+01	3.95E+00	7.83E+01	1.55E+00
(9,1)	1.03E+01	1.60E+00	9.74E+00	2.47E+00	1.09E+01	1.56E+00

B Rough estimation of the relative excess ground state bleach by spectral integration

In ref [9], it has been shown that charge carriers on (6,5) tubes cause two photoinduced absorption bands, PA_C and PA_T, respectively, and a concomitant reduction PB_C of the absorption of the S_{11} excitonic resonance of the neutral (6,5) tube, such that $PB_C = S_{11}(neutral) - S_{11}(charged) = PA_C + PA_T$. Transferring this finding to transient absorption (TA) spectroscopy, we can conclude that the contribution of photoinduced charges to the TA spectral integral is zero:

$$a_C^{6,5} = \int_\omega (\Delta A)_C^{6,5} d\omega = a(PA_C^{6,5}) + a(PA_T^{6,5}) + a(PB_C^{6,5}) = 0 \quad \text{(S1)}$$

Herein, $a(X) = \int_\omega X d\omega$ is the spectral integral of a photoinduced band X. Assuming that the validity of eq. S1 can be extended to all chiralities, we find

$$a_C^{tot} = \sum_{n,m} \int_\omega (\Delta A)_C^{n,m} d\omega = 0 \quad \text{(S2)}$$

This particular property of the optical probes of charged states (for probe energies around the S11 exciton resonance) allows us to ascribe any non-zero spectral integral to the presence of neutral photoexcitations of either singlet or triplet character:

$$a_n^{tot} = \int_\omega \Delta A d\omega \quad \text{(S3)}$$

Assuming now that the one-dimensional correlation lengths of neutral and charged excitations along the SWNTs are comparable, we can find the time-resolved ratio of neutral photoexcitations by comparing the excess (uncompensated) photobleach to the total photobleach:

$$r_N^{tot} = a_N^{tot} / \sum_{n,m} PB_{tot}^{n,m} \quad \text{(S4)}$$

The total photobleach can be approximated by integrating over the negative parts of the TA spectra only:

$$\sum_{n,m} PB_{tot}^{n,m} \geq \int_\omega 1/2 \cdot (\Delta A - |\Delta A|) d\omega \,, \quad \text{(S5)}$$

where the equal sign holds for negligible spectral overlap between negative and positive photoinduced bands.

We note that this formalism does so far not allow to obtain quantitative information on absolute triplet concentrations and yields; to this end the one-dimensional correlation length of the triplet state must be known. Nonetheless, due to the fact that this unknown quantity is not supposed to change on a long picosecond time scale, we can still use the formalism to describe the kinetics of transfer phenomena with relatively high precision.

C Nano-microsecond transient absorption spectra

For maximum reliability, we recorded TA spectra in the nanosecond to microsecond time regime in the same beamline as the femtosecond to picosecond spectra, which means that TA spectra across the full time range have been recorded with the same probe pulse, on the same day and the same spot on the sample, replacing only the femtosecond pulse by a 300 picosecond 532 nm pulsed laser as the pump source. We controlled the pump-probe delays electronically via a BNC (Model 575 Pulse/Delay Generator). Fig.S2 shows the typical TA spectra measured in pump-probe delays from nanoseconds to microseconds.

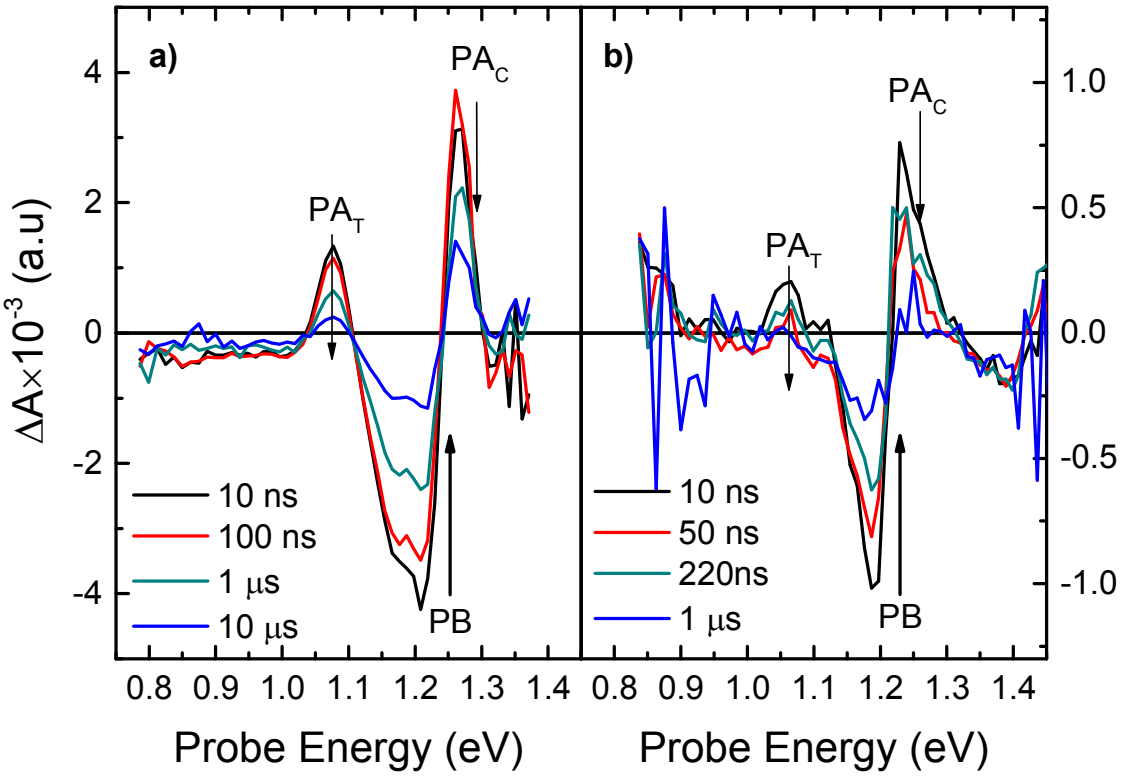

Fig.S2 Transient absorption spectra of (6,5) rich and (7,5) rich sample (left and right column, respectively) in pump-probe delays from nanoseconds to microseconds. Arrows next to PA and PB bands indicate the direction of evolution with increasing pump-probe delay. PB, PA_T and PA_C represent the photobleach, photoinduced trion band and photoinduced charge band.

D Global Spectral Modeling

Global spectral modeling of the TA spectra is performed with a custom-built software, in which a python script wraps around open source packages for matrix algebra (numpy) and nonlinear optimization (scipy). TA spectra after 50ps pump-probe delay are chosen for spectral modelling, in order to avoid strong contributions from singlet excitons, (see Fig. 1 in the main paper). We include only the (6,5) and (7,5) chiralites in the spectral model for the (6,5) rich sample, while (6,5), (7,5) and (8,4) are included for (7,5) rich sample. The main reasons for including those certain chiralities in the model but not all are: i) those are the main contributors in both ground

state absorption and TA spectra (see Fig. S1); ii) except (9,1) in (6,5) rich samples, the E11 transition bands of all other chiralities in both samples lie below those of (8,4), and their respective trion (PA_T) bands might reside outside of our measurement window, which adds difficulties on quantifying the excess PB we needed for further analysis of the TA spectra. In the model, only the main chirality ((6,5) in the (6,5) rich sample, and (7,5) in the (7,5) rich sample) produces a PB, a PA_T and a blueshifted photoinduced charge (PA_C) band, whereas each other chirality produces just a PB, as we do not see any signature of rising $PA_T^{7,5}$ in the TA spectra of (6,5) rich sample, although the $PB^{7,5}$ increases a lot in time. Then we apply a Gaussian line shape with specific parameters for all bands, and combine them to reproduce the complete TA spectra. The parameters for PB can be determined directly from the ground state absorption spectra, or from the actual TA spectra at early times, as they usually coincide very well. The necessary parameters for $PA_T^{6,5}$ and $PA_C^{6,5}$ have been taken from the global fit result of ground state absorption spectra of electrochemically doped similarly prepared SWNT sample, see Fig.S3. In that study, a set of ground state spectra, recorded at various doping levels, is reproduced quite well just with three spectral components namely undoped, moderately doped and heavily doped spectra [9]. For our purpose of spectral modeling here, we only use the moderately doped one, because it exhibits a $PA_T^{6,5}$ band around 1.06eV and a $PA_C^{6,5}$ around 1.27eV (see Fig.S3), and we assume that spectral doping of SWNTs with the pump pulse in the pump-probe experiment may induce a similar effect. To avoid inconsistency, we fit a set of TA spectroscopy data taken at different pump intensities with a whole range of pump-probe delays at once, with just a single model. Neither line width nor band center are allowed to change with pump intensities, so that any pump intensity dependent spectral features could be observed directly. Obtained best fit parameters are given in Table S3. The final outcome of the global spectral modeling would be the contribution of different excited state species on the TA spectra at certain times. In other words, it gives information about the population dynamics of excited states.

Table S3. Best spectral fit parameters obtained for (7,5) rich sample. In the table, rel.sp.wt stands for relative spectral weights, and is dimensionless, the rest are in (eV).

$PB^{6,5}$ center	$PB^{6,5}$ width	$PA_C^{6,5}$ center	$PA_C^{6,5}$ width	$PA_C^{6,5}$ rel.sp.wt	$PA_T^{6,5}$ center	$PA_T^{6,5}$ width	$PA_T^{6,5}$ rel.sp.wt	$PB^{7,5}$ center

1.25	0.05	1.274	0.07	0.57	0.065	0.041	0.43	1.195

Adapting the parameters for linewidth, band center and the spectral weight ratio of $PA_C^{6,5}$ and $PA_T^{6,5}$ from Fig. S3 for our model yields very nice global spectral fit result (see Fig.S4) with reliable time dependent spectral weights (Fig.S5)

In the case of (7,5) rich sample, we don't have similar electrochemical data as for (6,5). But we assume the parameters to be not very different from those of (6,5) rich sample, except the locations of the bands. Then we take the offsets between $PB^{6,5}$ and $PA_c^{6,5}$, $PB^{6,5}$ and $PA_T^{6,5}$ from the (6,5) rich sample to determine the band centers of the $PA_C^{7,5}$ and $PA_T^{7,5}$ in the (7,5) rich sample. The rest of the parameters are set to the same values as for the (6,5) rich sample. Fig. S6 and Fig. S7 show the results of spectral modeling and the corresponding population dynamics, respectively. Again the model reproduces the TA spectra quite well, except the PA signal around 1.33eV, Possibly because of the neglect of the (9,1) chirality in our spectral model.

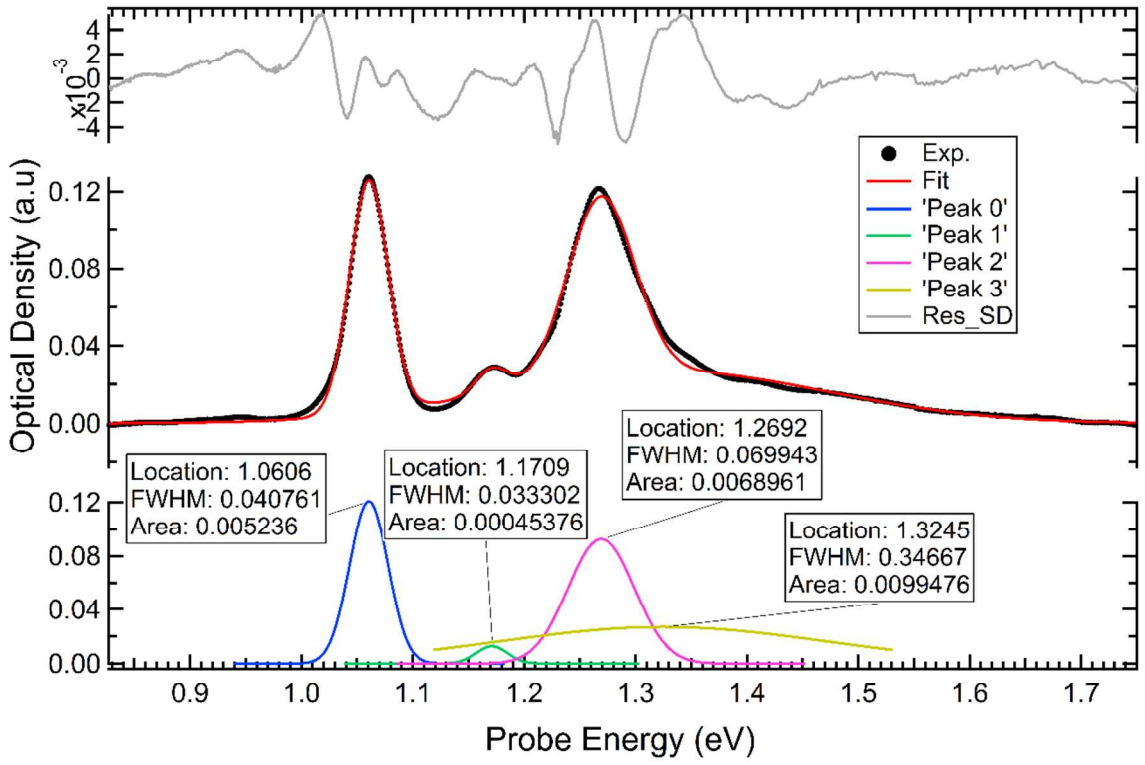

Fig.S3 Moderately doped spectra obtained from global analysis of ground state absorption spectra of (6,5) rich SWNTs recorded at various electrochemical doping levels [9]. Gaussian line shapes are applied

for all four bands, and parameters of only the 'Peak 0' and 'Peak 2' are used for $PA_T^{6,5}$ and $PA_C^{6,5}$ in spectral modeling, as the other two peaks are originated from different chiralities.

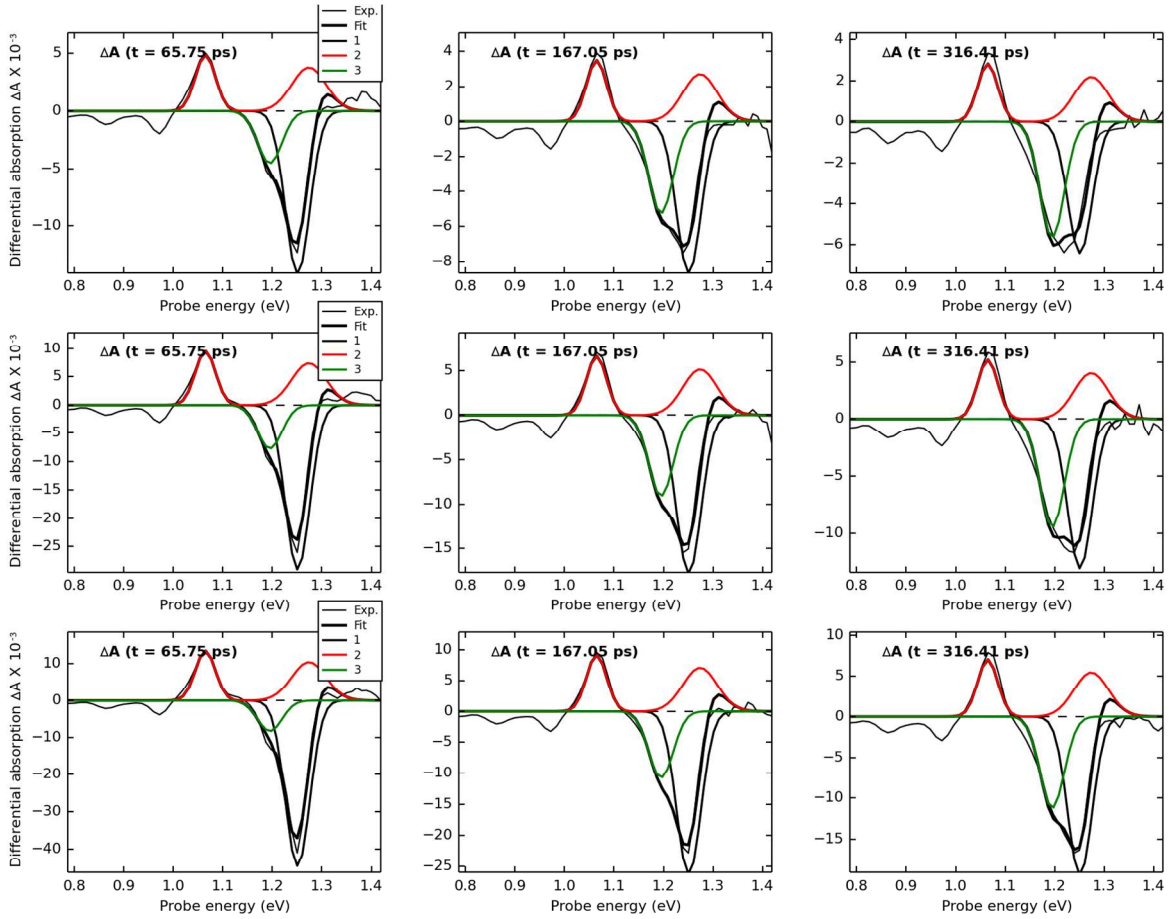

Fig.S4 Representative figures for the result of global spectral modeling on the TA spectra of the (6,5) rich sample. Each column represents different pump-probe delays, while each row represents different pump energy densities, 33, 99, 198$\mu J/cm^2$, respectively. The black, red and green lines marked as 1, 2 and 3 are $PB^{6,5}$, $PA_C^{6,5} + PA_T^{6,5}$ and $PB^{7,5}$. The PBs around 0.97eV and 0.87eV are not fitted because, as reasoned earlier in the text, the corresponding chiralities were not included in the model.

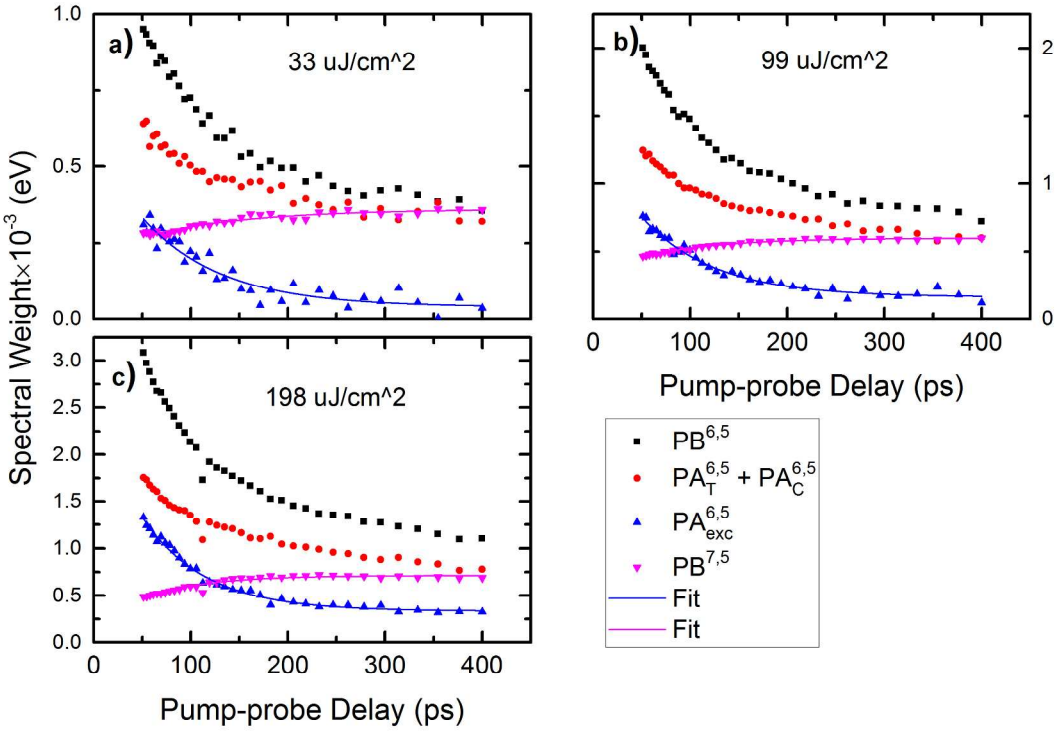

Fig.S5 Population dynamics of excited states in (6,5) rich SWNT sample after 50ps of pump-probe delay, achieved by global spectral modeling of TA spectra, with three different pump energy densities. $PB_{exc}^{6,5}$ *is obtained by subtracting the sum of (6,5) charged states* $(PA_T^{6,5} + PA_C^{6,5})$ *from the total* $PB^{6,5}$.

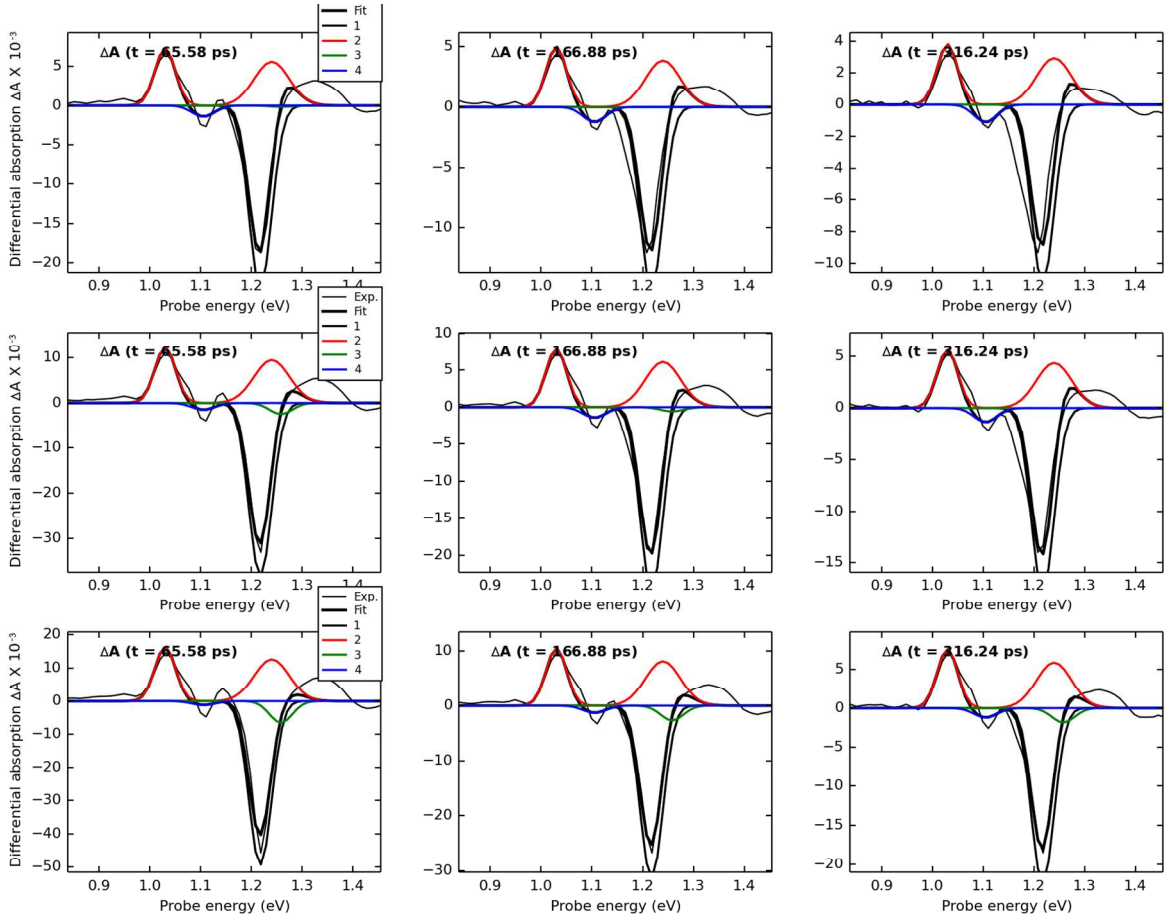

Fig.S6 Representative figures for the result of global spectral modeling on the TA spectra of the (7,5) rich sample. Each column represents different pump-probe delays, while each row represents different pump energy densities, 33, 99, 198$\mu J/cm^2$, respectively. The black, red and green and blue curves marked as 1, 2, 3 and 4 are the $PB^{7,5}$, sum of (7,5) charged states ($PA_T^{7,5} + PA_C^{7,5}$) , $PB^{6,5}$ and $PB^{8,4}$, respectively.

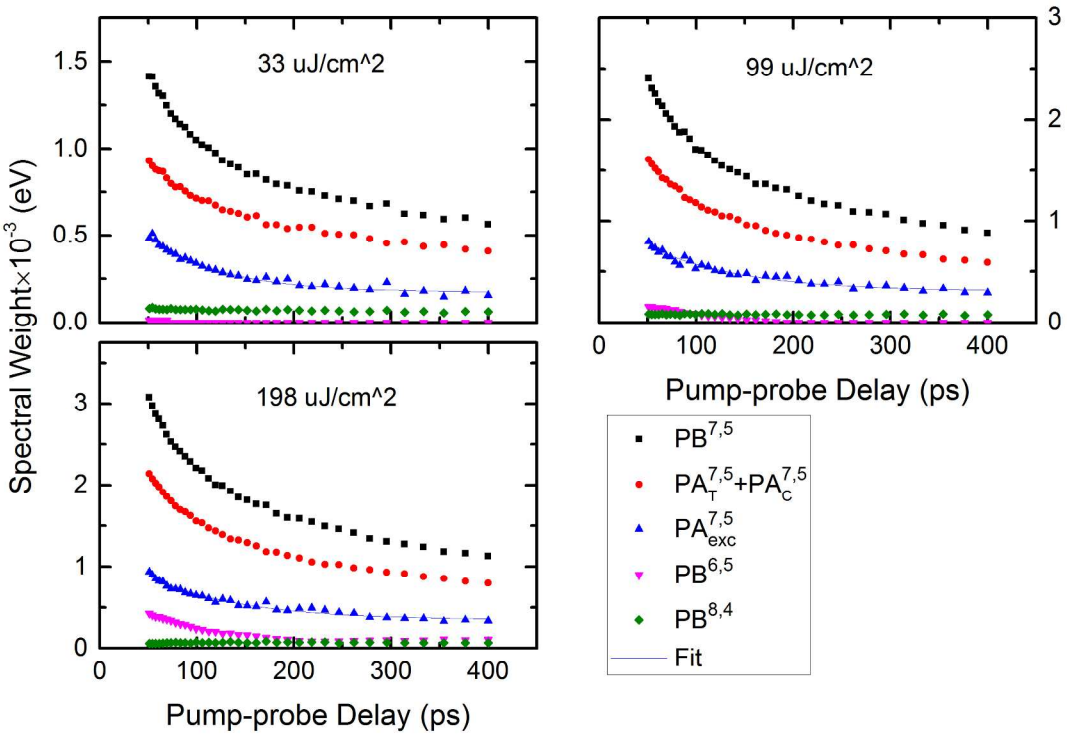

Fig.S7 Population dynamics of excited states in (7,5) rich SWNT sample after 50ps of pump-probe delay, achieved by global spectral modeling of TA spectra, with three different pump energy densities. $PB_{exc}^{7,5}$ *is obtained by subtracting the sum of (7,5) charged states* $(PA_T^{7,5} + PA_C^{7,5})$ *from the total* $PB^{7,5}$.

References

(1) Kim, W.-J.; Lee, C. Y.; O'brien, K. P.; Plombon, J. J.; Blackwell, J. M.; Strano, M. S., Connecting Single Molecule Electrical Measurements to Ensemble Spectroscopic Properties for Quantification of Single-Walled Carbon Nanotube Separation. *J. Am. Chem. Soc.* **2009**, *131*, 3128-3129.

(2) Park, J.; Deria, P.; Olivier, J.-H.; Therien, M. J., Fluence-Dependent Singlet Exciton Dynamics in Length-Sorted Chirality-Enriched Single-Walled Carbon Nanotubes. *Nano Lett.* **2014**, *14*, 504-511.

(3) Grechko, M.; Ye, Y.; Mehlenbacher, R. D.; McDonough, T. J.; Wu, M.-Y.; Jacobberger, R. M.; Arnold, M. S.; Zanni, M. T., Diffusion-Assisted Photoexcitation Transfer in Coupled Semiconducting Carbon Nanotube Thin Films. *ACS Nano* **2014**, *8*, 5383-5394.

(4) Lüer, L.; Crochet, J.; Hertel, T.; Cerullo, G.; Lanzani, G., Ultrafast Excitation Energy Transfer in Small Semiconducting Carbon Nanotube Aggregates. *ACS Nano* **2010**, *4*, 4265-4273.

(5) Koyama, T.; Miyata, Y.; Asaka, K.; Shinohara, H.; Saito, Y.; Nakamura, A., Ultrafast Energy Transfer of One-Dimensional Excitons between Carbon Nanotubes: A Femtosecond Time-Resolved Luminescence Study. *Phys. Chem. Chem. Phys.* **2012**, *14*, 1070-1084.

(6) Koyama, T.; Miyata, Y.; Asada, Y.; Shinohara, H.; Kataura, H.; Nakamura, A., Bright Luminescence and Exciton Energy Transfer in Polymer-Wrapped Single-Walled Carbon Nanotube Bundles. *J. Phys. Chem. Lett.* **2010**, *1*, 3243-3248.

(7) Yuma, B., et al., Biexciton, Single Carrier, and Trion Generation Dynamics in Single-Walled Carbon Nanotubes. *Phys. Rev. B* **2013**, *87*, 205412.
(8) Styers-Barnett, D. J.; Ellison, S. P.; Mehl, B. P.; Westlake, B. C.; House, R. L.; Park, C.; Wise, K. E.; Papanikolas, J. M., Exciton Dynamics and Biexciton Formation in Single-Walled Carbon Nanotubes Studied with Femtosecond Transient Absorption Spectroscopy. *J. Phys. Chem. C* **2008**, *112*, 4507-4516.
(9) Hartleb, H.; Späth, F.; Hertel, T., Evidence for Strong Electronic Correlations in the Spectra of Gate-Doped Single-Wall Carbon Nanotubes. *ACS Nano* **2015**, *9*, 10461-10470.